CrossMark

J. Fluid Mech. (2016), *vol.* 801, *pp.* 250–259. © Cambridge University Press 2016
doi:10.1017/jfm.2016.432

Holes stabilize freely falling coins

Lionel Vincent[1], **W. Scott Shambaugh**[1] **and Eva Kanso**[1,†]

[1]Department of Aerospace and Mechanical Engineering, University of Southern California, Los Angeles, CA 90089, USA

(Received 7 December 2015; revised 2 March 2016; accepted 20 June 2016; first published online 21 July 2016)

The free fall of heavy bodies in a viscous fluid medium is a problem of interest to many engineering and scientific disciplines, including the study of unpowered flight and seed dispersal. The falling behaviour of coins and thin discs in particular has been categorized into one of four distinct modes; steady, fluttering, chaotic or tumbling, depending on the moment of inertia and Reynolds number. This paper investigates, through a carefully designed experiment, the falling dynamics of thin discs with central holes. The effects of the central hole on the disc's motion is characterized for a range of Reynolds number, moments of inertia and inner to outer diameter ratio. By increasing this ratio, that is, the hole size, the disc is found to transition from tumbling to chaotic then fluttering at values of the moment of inertia not predicted by the falling modes of whole discs. This transition from tumbling to fluttering with increased hole size is viewed as a stabilization process. Flow visualization of the wake behind annular discs shows the presence of a vortex ring at the disc's outer edge, as in the case of whole discs, and an additional counter-rotating vortex ring at the disc's inner edge. The inner vortex ring is responsible for stabilizing the disc's falling motion. These findings have significant implications on the development of design principles for engineered robotic systems in free flight, and may shed light on the stability of gliding animals.

Key words: flow–structure interactions, instability, swimming/flying

1. Introduction

Objects falling freely under gravity through a fluid medium may follow various periodic or chaotic paths depending on their geometry, the ratio of the disc to fluid density and the fluid viscosity. Understanding the origin and nature of these non-straight paths is relevant to many branches of science and engineering. Examples range from seed dispersal (Lentink *et al.* 2009; Lentink & Biewener 2010) and insect flight (Andersen, Pesavento & Wang 2005) to fish swimming (Gazzola *et al.* 2011) and marine engineering (Williamson & Govardhan 2004).

Coins, or more precisely, thin discs, are the simplest three-dimensional shapes that afford non-straight descent paths, and as such have been the subject of intensive research, see, e.g., Ern *et al.* (2012) for a brief review. It is well established that a thin

†Email address for correspondence: kanso@usc.edu

https://doi.org/10.1017/jfm.2016.432 Published online by Cambridge University Press

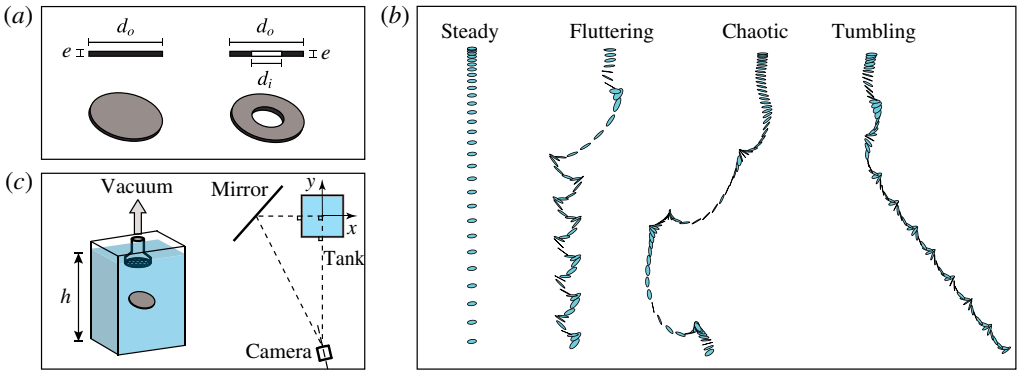


FIGURE 1. (Colour online) (*a*) Discs without and with central holes. (*b*) A disc without a central hole falling in a fluid medium adopts one of the four well-defined regimes: steady, fluttering, chaotic and tumbling (adapted from Heisinger, Newton & Kanso 2014). We investigate how the addition of a central hole affects the disc's motion, by methodically varying the annular aspect ratios d_i/d_o of the disc while keeping its thickness e constant. (*c*) Experimental apparatus: discs are released from rest, and their dynamic is probed using three-dimensional trajectory reconstruction and digital particle image velocimetry (PIV).

disc falls in one of four distinct descent modes; steady, fluttering, chaotic or tumbling. Field *et al.* (1997) mapped out the regions associated with these four descent modes in a two-dimensional parameter space consisting of the disc's dimensionless moment of inertia I and the ratio of fluid inertial to viscous forces reflected by the Reynolds number Re. More recently, Auguste, Magnaudet & Fabre (2013) used a numerical approach to construct a parameter space using I and the Archimedes number Ar, which is essentially a Reynolds number based on a settling velocity obtained by balancing inertial drag and gravity. In a Focus on Fluids letter, Moffatt (2013) reviewed the results of Auguste *et al.* (2013) and contemplated what the effects of other parameters, such as surface roughness, central hole or wavy edge, would be on the disc's descent modes. Moffatt speculated that, compared with whole discs, annular discs would have different wakes, which would in turn affect the instabilities underlying their descent modes.

In this paper, we investigate experimentally the falling modes of annular discs and compare them to whole discs (see figure 1). For annular discs, one has six material parameters: the disc's outer diameter d_o, inner diameter d_i, thickness e and density ρ_d, as well as the fluid density ρ_f and kinematic viscosity ν. The height h from which the disc is dropped is used to determine the mean vertical velocity $U = h/T$, where T is the total travel time, i.e. the time the disc takes to reach the bottom of the tank from its initial height h, and it is not known *a priori*. From these dimensional quantities, five independent dimensionless parameters may be formed: the dimensionless moment of inertia $I = I_{disc}/\rho_f d_0^5 = (\pi e \rho_d/64 d_o \rho_f)(1 - (d_i/d_o)^4)$, the Reynolds number $Re = U(d_o - d_i)/\nu$ and the ratios d_i/d_o, e/d_o and h/d_o. It should be emphasized that this choice of I and Re depends on the non-dimensional parameter d_i/d_o, and thus accounts for the presence of the hole in the coin.

For the discs considered here, e/d_o is small (less than 0.1) and thus plays negligible role in the dynamics. The height h/d_o from which the discs are dropped is chosen to be sufficiently large ($h/d_o > 20$) to allow the falling regime to fully develop during the observation window. Therefore, the annular discs considered in this study are

https://doi.org/10.1017/jfm.2016.432 Published online by Cambridge University Press

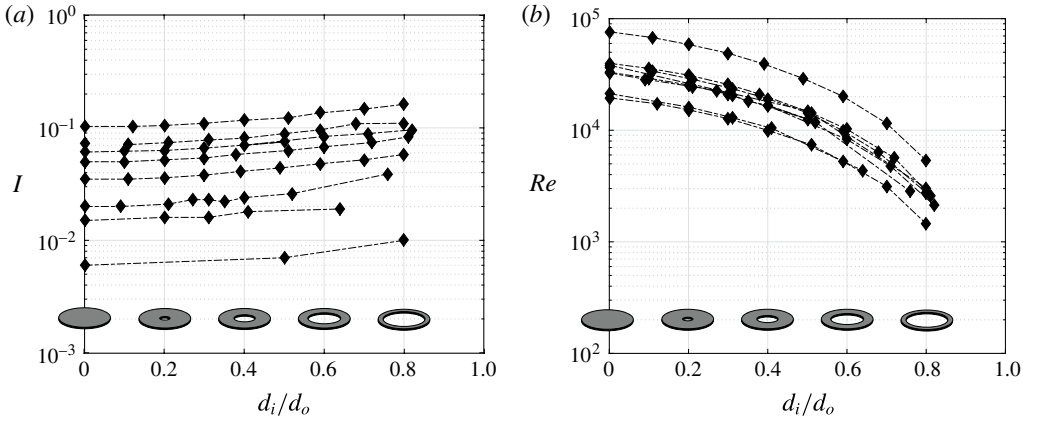


FIGURE 2. Discs considered in this study: their parameters in the $(d_i/d_o, I)$ and $(d_i/d_o, Re)$ planes, respectively. Here, $I = (\pi e \rho_d / 64 d_o \rho_f)(1 - (d_i/d_o)^4)$ compares the disc's moment of inertia to that of the fluid while the Reynolds number $Re = U(d_o - d_i)/\nu$ is based on the average downward velocity U.

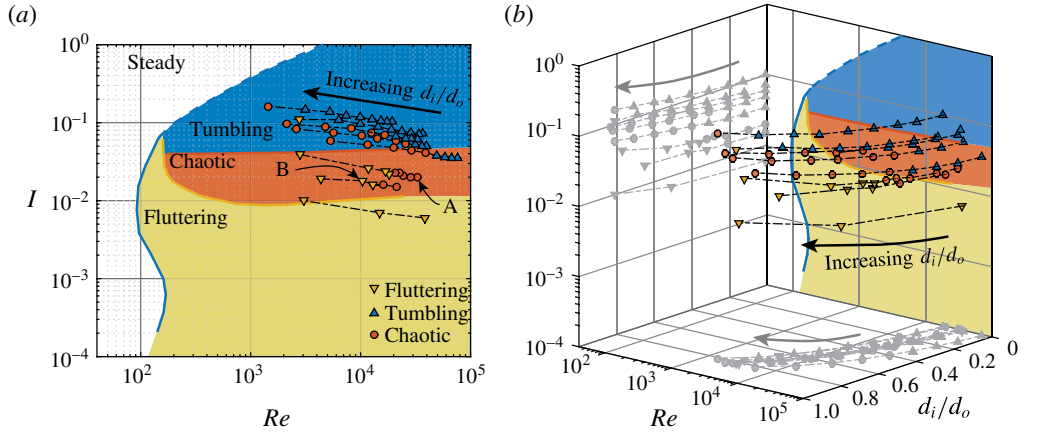


FIGURE 3. (Colour online) (*a*) The parameter space (I, Re) of Field *et al.* (1997) for discs with no holes $(d_i/d_o = 0)$ is reproduced here. The yellow region corresponds to fluttering, red to chaotic and blue to tumbling. Superimposed on this space are the data points from our experimental study of discs with central holes. Arrows labelled A and B show the location of the two discs used in figure 4. (*b*) Three-dimensional parameter space $(I, Re, d_i/d_o)$.

characterized by a three-dimensional parameter space $(I, Re, d_i/d_o)$. The parameter values considered in this study are depicted in figure 2.

When $d_i/d_o = 0$, we recover the case of whole discs considered in Field *et al.* (1997), Heisinger *et al.* (2014). In this case, a visualization of the four falling modes is reprinted from Heisinger *et al.* (2014) in figure 1(*b*). The three-dimensional positions and orientations of the discs are reconstructed from high-speed photography using the set-up shown in figure 1(*c*). For $d_i/d_o = 0$, the parameter space (I, Re) in figure 2 of Field *et al.* (1997) is reproduced in figure 3(*a*). When viscous forces dominate ($Re < 90$), a disc released with zero (or close to) zero initial conditions

https://doi.org/10.1017/jfm.2016.432 Published online by Cambridge University Press

falls downwards in a 'steady' motion without induced instabilities, regardless of I. When inertial forces dominate ($Re > 800$), a disc's motion depends largely on I. At high I (approximately $I \geqslant 4 \times 10^{-2}$), after a period of transient motion, the disc will auto-rotate end over end in a tumbling motion. At low I (approximately $I \leqslant 9.5 \times 10^{-3}$), the disc will settle into an oscillating fluttering motion. For $9.5 \times 10^{-3} \leqslant I \leqslant 3 \times 10^{-2}$, there is a transitional region between fluttering and tumbling where the disc will both oscillate and invert in a chaotic motion. Oscillations and inversions in a chaotic trajectory occur with equal probability, as manifested by the $\sim$50 % likelihood of landing 'heads up' obtained in Heisinger *et al.* (2014). The region of $90 < Re < 800$ is the intersection of the boundaries of the four falling mode regions, and behaviour in this region depends heavily on both I and Re.

Auguste *et al.* (2013) identified two additional descent modes that correspond to non-planar (gyrating) fluttering and tumbling, which they denoted hula hoop and helical auto-rotation, respectively. The domains of these falling modes, reported in the (I, Ar) space, can be mapped into subsets of the fluttering and tumbling regions in the parameter space (I, Re) of Field *et al.* (1997). However, the latter does not explicitly distinguish between planar and gyrating fluttering/tumbling. In Heisinger *et al.* (2014, figure 4(*a*,*b*)), the same disc subject to slightly different initial conditions dictated by the small uncertainty inherent in the disc-release mechanism is shown to exhibit either planar fluttering or hula hoop motion. Therefore, we feel that such distinction in the parameter space, while possible in a computational model with zero uncertainty in initial conditions, is more difficult experimentally.

Finally, we revisit the definition of what exactly 'thin' means. Field *et al.* (1997) focused on discs with $e/d_o \leqslant 0.1$, with the implicit assumption that a disc's falling behaviour is invariant with respect to e/d_o for smaller values. Auguste *et al.* (2013) challenged this assumption, finding approximately 15 %–20 % difference in Re marking the boundaries between the various falling regimes for discs with $e/d_o \leqslant 0.1$. In essence, they found that thinner discs are more unstable. However, their investigation was limited to $Ar \leqslant 110$ ($Re \leqslant 270$), where the falling mode has high dependence on Re. Here, we posit that the effect of e/d_o should be much lower in the $10^3 \leqslant Re \leqslant 10^5$ region we are investigating due to the aforementioned low dependence of the falling mode on Re for $Re > 800$. The discs used in this work are in the range of $1/13 \leqslant e/d_o \leqslant 1/660$.

The organization of this paper is as follows: a description of the experimental methods is given in § 2 and the obtained results are described in § 3. The implications of this findings on passive flight are discussed in § 4.

2. Methods

In order to investigate how the presence of a central hole, i.e. non-zero d_i/d_o, affects the falling mode of the disc, we needed to design discs that span a subset of the parameter space $(I, Re, d_i/d_o)$. One way to approach this task is to fix the disc's thickness e and outer diameter d_o and vary d_i, which answers the practical question, 'what happens if I take a given disc and drill a hole in its centre?' However, this approach would cause a simultaneous decrease in the value of I, making it difficult to isolate the effect of decreasing I from that of increasing d_i/d_o. The ideal approach would be to hold I and Re constant while varying d_i/d_o. However, this approach posed problems for manufacturing: for $d_i/d_o > 0.5$, discs became too large to manufacture with available machining methods. The approach we used is to fix e and vary d_i and d_o simultaneously such that I is almost constant. The values of $(I, d_i/d_o)$ that we

https://doi.org/10.1017/jfm.2016.432 Published online by Cambridge University Press

explored in this study are depicted in figure 2(*a*). This manufacturing approach causes a drift towards lower *Re*, as shown in figure 2(*b*). The drift line, when viewed in the parameter space (I, Re) depicted in figure 3(*a*), is roughly parallel to the boundaries delineating the transition between the falling modes. Because the falling modes of regular discs are largely independent of the Reynolds number for $Re \geqslant 800$, we can practically disregard the effect of *Re* for discs in the range $10^3 \leqslant I \leqslant 10^5$, and focus on the effects of varying I and d_i/d_o only. Note that, in order to offset the effect of decreasing *Re* and ensure that as d_i/d_o increases, the disc parameters change such that the data points in the (I, Re) space are roughly parallel to the transition boundaries, not crossing them, we imposed a small drift upward in the values of I.

Because the velocity U was not known *a priori*, to estimate *Re* during the design process, we used the terminal velocity V_t of a buoyant object falling in a fluid. The terminal velocity V_t is given by $V_t = \sqrt{2(\rho_d/\rho_f - 1)ge/C_d}$, where the drag coefficient C_d of each disc was determined from the model of Roger & Hussey (1982). Once the disc's descent motion was obtained, we adjusted the value of *Re* based on the computed velocity U. To ensure sufficient data points in the (I, d_i/d_o) plane and achieve parameter values within those mapped out by Field *et al.* (1997), we used different disc materials in two fluid mediums. Namely, the pairings we used are steel ($\rho_d = 7790 \pm 10$ kg m^{-3}) in water, cardstock ($\rho_d = 813 \pm 8$ kg m^{-3}) in air and foam-core board ($\rho_d = 111.3 \pm 0.7$ kg m^{-3}) in air.

In all experiments, the discs were released with zero initial conditions using a release mechanism that employs active suction and is capable of accommodating discs with a wide range of sizes and materials (see figure 1*c*). When the suction is turned off, the pressure difference holding the disc vanishes and the disc falls. To determine the uncertainty inherent in the release mechanism and hence, the repeatability of the initial conditions, we used the release mechanism to drop a steel ball 30 times. A steel ball was used to avoid the effects of the flow-induced instabilities underlying the discs' falling modes. The steel ball consistently landed right beneath the dropping point with a deviation within 0.9 % of the vertical drop distance h.

Each disc was dropped 5 times from a height that allowed its final falling mode to fully develop and be observed. Every disc exhibited a consistent falling mode over all trials. The discs' falling trajectories were recorded with a high-resolution camera (Point Grey Grasshopper3). Images were acquired simultaneously from the front and the side using a properly positioned mirror, see figure 1(*c*), allowing three-dimensional trajectory reconstruction using an in-house algorithm. Moreover, we used particle image velocimetry to locally investigate the fluid motion around the disc at the onset of motion. Here, the water tank was seed with 200-um Pliolite particles and a vertical laser was used to illuminate the mid-section of the particle-seeded tank. Images were recorded using a Phantom M-110 high-speed camera and processed with the open-source MATLAB app PIVlab (see Thielicke & Stamhuis 2014).

3. Results

We examine the falling modes of the discs whose parameter values are shown in figure 2. The discs for which $d_i/d_o = 0$ are used to validate the experimental protocol. All these discs, but one, exhibited falling modes that are consistent with those predicted by the parameter space (I, Re) of Field *et al.* (1997). The one exception occurs at approximately $I = 3.5 \times 10^{-2}$ and $Re = 7.6 \times 10^4$, that is, at *Re* larger than the maximum value $Re = 3 \times 10^4$ reported in Field *et al.* (1997). This suggests that, for whole discs, the roughly flat, horizontal boundary between the tumbling and

https://doi.org/10.1017/jfm.2016.432 Published online by Cambridge University Press

chaotic modes may curve downwards at higher Re. Although a full investigation of this region of the (I, Re) space is outside the scope of the present study, we note that the change in falling mode at $Re = 7.6 \times 10^4$ is reminiscent of the sudden change in aerodynamic properties (drag crisis) observed for regularly shaped objects such as spheres at $Re \sim 10^5$ (see, e.g. Landau & Lifschitz (1987), p. 181). For this value of Re, the boundary layer and wake become fully turbulent. The free fall of discs with fully turbulent wakes remains an open research question, as pointed out by Moffatt (2013).

Figure 3 shows a classification of the descent modes of all discs into fluttering (yellow downward-pointing triangles), chaotic (red circles), and tumbling (blue upward-pointing triangles). This classification is superimposed on the parameter space (I, Re) of Field *et al.* (1997) in figure 3(*a*) whereas the three-dimensional parameter space $(I, Re, d_i/d_o)$ is shown in figure 3(*b*). One can readily observe that increasing the aspect ratio d_i/d_o has a stabilizing effect on the disc's falling motion. For roughly the same I, tumbling discs transition into a chaotic falling mode at higher d_i/d_o and chaotic discs transition into a fluttering motion.

Most of the transitions between falling modes are seen at $d_i/d_o = 0.3 \pm 0.1$. For smaller I, it takes smaller values of d_i/d_o to cause a transition in the falling behaviour. This suggests that increasing the annular ratio d_i/d_o while holding I constant can be thought of as having the same effect as decreasing I while holding Re constant (for sufficiently large Re). In the latter, the falling mode changes from tumbling to chaotic then fluttering. A similar sweep from tumbling to chaotic then fluttering can be seen along the $I = 4 \times 10^{-2}$ line as d_i/d_o increases. The four tumbling discs that lay just beneath the tumbling–chaotic boundary and are an exception to this trend, are the discs with higher Re than those explored by Field *et al.* (1997).

In an effort to understand the mechanism responsible for this change in behaviour, we used flow visualization and PIV to investigate the flow field around the disc shortly after the onset of motion. Figure 4(*a*) shows the trajectory of a regular disc ($d_i/d_o = 0$) falling in the chaotic regime. The Reynolds number and moment of inertia are $Re = 3.3 \times 10^4$ and $I = 20 \times 10^{-3}$, respectively. The associated flow field shortly after the disc is released into the flow is depicted in figure 4(*b*). A single vortex ring develops in the disc's wake, and is then shed as the disc drifts sideways. Figure 4(*c*) shows the trajectory of a disc with central hole $d_i/d_o = 0.4$, $I = 18 \times 10^{-3}$, and $Re = 1.0 \times 10^4$. Note that for these values of I and Re, a disc with no hole would be in the chaotic regime. In contrast, the disc with central hole falls in a very clear planar, fluttering motion, as indicated by the top view in the inset of figure 4(*c*). The flow field (figure 4*d*) shows again a vortex ring around the outer edge, similarly to the whole disc case. In addition to the vortex ring at the outer edge, a counter-rotating secondary vortex ring develop along the inner edge of the central hole. The combined action of the outer and inner vortex rings induce a stabilizing downward momentum acting on the full surface of the annular disc.

We then examined quantitatively the circulation of the shed vortices. To this end, we performed PIV experiments. Figures 5(*a*) and 5(*b*) show snapshots of the flow velocity and vorticity field for the two coins shown in figure 4. We considered a number of full coins in the chaotic and fluttering regime, with the following parameter values: $I = 0.006$, 0.0152, 0.020, 0.025 and 0.033 and Re ranging from 14×10^3 to 26×10^3. In each case, we characterized systematically the time-dependent vortex circulation, from the onset of motion to the first vortex shedding event. For full coins, one has only one vortex ring of total circulation Γ_o; see schematic depiction in the bottom left of figure 5(*c*). We scaled time and circulation using the gravitational time scale

https://doi.org/10.1017/jfm.2016.432 Published online by Cambridge University Press

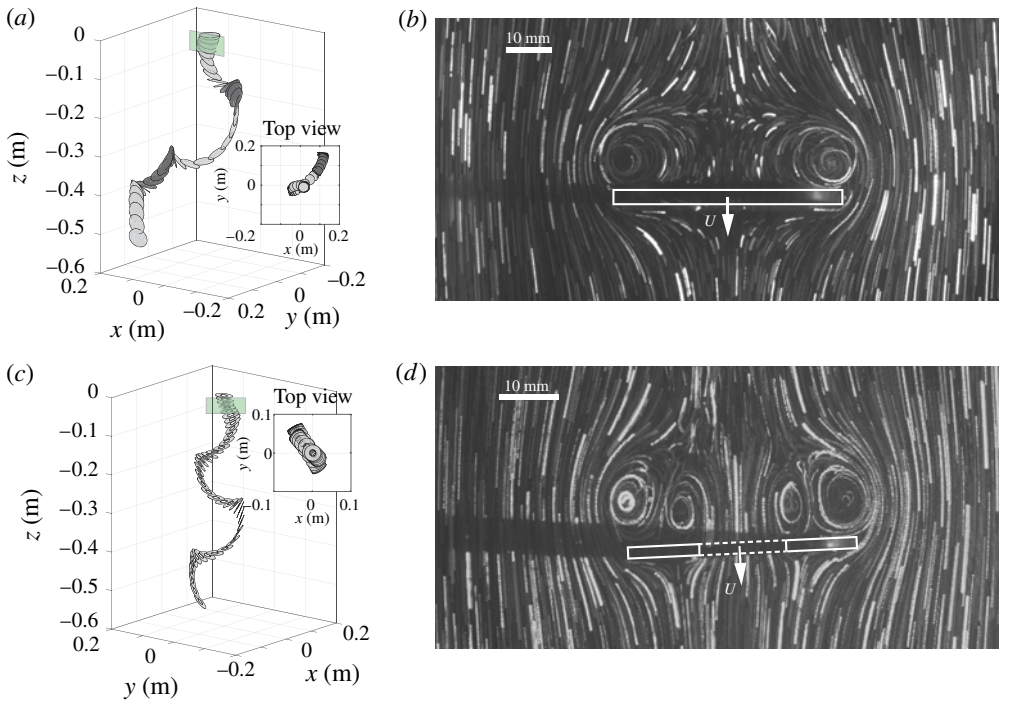


FIGURE 4. (Colour online) (*a*) Chaotic trajectory of disc with no hole: $d_i/d_o = 0$, $Re = 3.3 \times 10^4$ and $I = 20 \times 10^{-3}$. (*b*) Visualization of the flow field around the coin in its own reference frame, shortly after release. (*c*) Fluttering trajectory of disc with central hole: $d_i/d_o = 0.4$, $Re = 1.0 \times 10^4$ and $I = 18 \times 10^{-3}$. (*d*) Flow field. Exposure time is 40 ms for both images. The presence of a hole favours the generation of a secondary smaller vortex ring, stabilizing the coin's falling motion.

$\sqrt{d_o/g}$ and corresponding circulation scale $d_o\sqrt{gd_o}$. The vortex circulation grows linearly with time (figure 5*c*) in agreement with previous computational observations on falling plates (Mittal, Seshadri & Udaykumar 2004; Michelin & Llewellyn-Smith 2009). It should be noted that as the moment of inertia I increases, circulation increases accordingly in a linear fashion. In figure 5(*c*), we highlighted the transition between the fluttering to chaotic regimes in figure 5(*c*) by direct comparison to figure 3. The transition occurs at $I \simeq 0.012$ and is essentially independent of Re for $Re \sim 10^4$.

We compared the circulation of the full coins to that of the coin with hole presented in figure 4 for which $I = 0.018$ and $d_i/d_o = 0.4$, and $Re = 10 \times 10^3$. Here, two attached vortex rings are present at all time: the outside vortex ring, with associated circulation Γ_o and the inner vortex ring, with circulation Γ_i in the opposite direction. We noticed that the centre of the outer vortex ring is located close to the outer edge (same as the full coin case) and that of the inner ring is located close to the inner edge. Therefore, we compute the equivalent vorticity as $\Gamma = \Gamma_o - (d_i/d_o)\Gamma_i$, as a way to account for the difference in 'lever arm'. The resulting circulation is depicted in figure 5(*c*), open triangles. Clearly, the circulation is not growing in a strict linear fashion: it depends on the balance between the outside vortex ring, which grows as t and the inner vortex ring which grows closer to t^2 at short time. More importantly, the value of the circulation is twofold lower than the expected value for a full coin

https://doi.org/10.1017/jfm.2016.432 Published online by Cambridge University Press

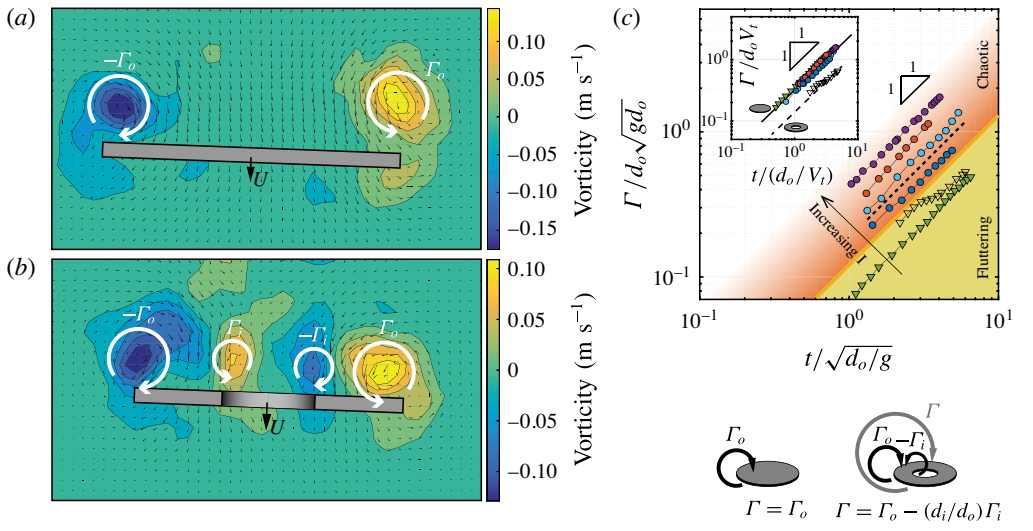


FIGURE 5. (Colour online) PIV-based quantification of vortex circulation at the onset of the path instability. (*a*,*b*) Velocity flow field and corresponding vorticity of the two coins used in figure 4. (*c*) Vortex circulation dominates the coin's dynamics at short times and increase linearly with time for full coins (filled symbols). Increasing moment of inertia I results in higher circulation. For hollow coins (open triangles), the secondary smaller vortex ring induced by the presence of the hole decreases the overall circulation, and stabilizes the coin's decent; dash line shows the expected circulation for a full coin with the same I. (*c*, inset), Circulation versus time using the terminal velocity $V_t = \sqrt{2(\rho_d/\rho_f - 1)ge}$ as the velocity scale and rescaling the other quantities accordingly; solid line is given by $\Gamma/(d_oV_t) = 0.32 \pm 0.04t/(d_o/V_t)$. Parameters for the full coins are $I = 0.0060, 0.0152, 0.020, 0.025$ and 0.033 and Re in the range 14×10^3 to 26×10^3.

with same moment of inertia $I = 0.018$ (shown as a dashed line in 5*c*). In addition, the circulation value is comparable to the circulation of the fluttering full coin ($I = 0.0060$), suggesting that two objects with similar circulation will fall in the same regime. These results indicate that the descent mode may be dominated by the value of the net circulation in the vorticity of the coin.

Finally, we rescale time and circulation using the terminal velocity $V_t = \sqrt{2(\rho_d/\rho_f - 1)ge}$ in lieu of the gravitational velocity $\sqrt{gd_o}$, see inset of 5(*c*). The circulation data for the full coins collapse to a single master curve. To our knowledge, this is the first time this collapse of data has been reported in the literature. This collapse emphasizes the importance of the hydrodynamic effects, indicating a universal dependence of the circulation on the flow-based terminal velocity V_t rather than on the gravitational velocity $\sqrt{gd_o}$. In this rescaling, the coin with hole (open triangles) stands separately from the full coins, showing significantly lower circulation. As d_i/d_o increases further, we expect a decrease in the difference between the magnitude of the outer and inner vortex rings, and therefore we expect the total circulation $\Gamma = \Gamma_o - d_i\Gamma_i/d_o$ to decrease further.

4. Discussion

Coins and thin discs falling in a viscous medium have received a great deal of attention (see e.g. Ern *et al.* 2012), and their falling modes have been categorized

https://doi.org/10.1017/jfm.2016.432 Published online by Cambridge University Press

into steady, fluttering, chaotic and tumbling (Willmarth, Hawk & Harvey 1964; Field *et al.* 1997). This work investigated the effect of central holes on the falling motion of discs. Three dimensionless parameters were identified: the moment of inertia I, the Reynolds number Re and the ratio of inner to outer diameter d_i/d_o. This choice of dimensionless parameters is consistent with previous work on whole discs (Field *et al.* 1997) and allows for direct comparison between the falling motion of discs with holes and those without.

According to Field *et al.* (1997), at a given Re (for $Re > 800$), as I decreases, a whole disc transitions from tumbling to chaotic motion to fluttering. Interestingly, for discs with central holes, a similar transition from tumbling to chaotic then fluttering was obtained as we increased the size of the central hole. In other words, central holes stabilize the falling motion of discs. We view this transition for smaller I as a stabilization process for two physical reasons. Firstly, the fact that tumbling discs, depending on the height from which they are released, take large excursions away from their release location, whereas fluttering discs land close to their release location and never invert (see Heisinger *et al.* 2014). Secondly, a tumbling disk has more rotational kinetic energy than a disk falling in a chaotic fashion which in turn has more rotational kinetic energy than a fluttering disk. For discs with holes, the stabilization effect was not immediate for small aspect ratios d_i/d_o; it is rather gradual as d_i/d_o increases. For the range of Re considered, the hole size necessary to transition a disc from one falling mode to another is highly dependent on I. At higher I, many of the tumbling discs did not become chaotic until $d_i/d_o = 0.8$, and most did not exhibit fluttering behaviour at all. In some of these cases, fluttering may be attainable as d_i/d_o gets closer to 1, that is, for discs that are no more than thin rings.

Simulations by Mittal *et al.* (2004) peg the mechanism that oscillates rectangular plates falling through a fluid as the torque induced by vortex shed off from the plates' edges. As the strength of these vortices increase with larger I, the flow-induced torque becomes strong enough to eventually flip the oscillating plate and induce tumbling motion. The dominant contribution of the unsteady wake on the descent motion was also recognized by Jones & Shelley (2005), who computed the short-time dynamics of fluttering plates using a boundary integral technique. Here, we examined the flow field around whole and annular discs shortly after their release in order to shed light on the mechanisms responsible for stabilizing the annular discs. Our flow visualization show that whole discs have counter-rotating vortices at the outer edge of the disc, while annular discs have an additional pair of counter-rotating vortices on the disc's inner edge. Annular discs have essentially two counter-rotating vortex rings. The presence of the inner vortex ring explains the stabilization effect of central holes: the counter-rotating inner vortex weakens the net flow-induced torque on the disc. This weakening effect could be attributed to two reasons. First, as d_i/d_o increases, the length span along which the inner vortex ring acts (i.e. the circumference of the inner hole), approaches parity with the length span along which the outer vortex acts. In this way, the strength of the inner and outer vortex rings equalizes. The second explanation is that increasing d_i/d_o simply increases the length of the lever arm upon which the inner vortex is acting. A detailed analysis of contribution of each of these effects to the stabilizing mechanism will be explored in future research.

Based on our findings, one could envision the use of central holes as a strategy to stabilize the free fall of discs or disc-shaped passive flyers. This strategy is potentially most useful for discs that are close to the transition between two falling modes. In these cases, one could, through open loop or feedback control, change the falling mode by changing the size of the central hole and, in turn, control the landing

https://doi.org/10.1017/jfm.2016.432 Published online by Cambridge University Press

distribution and likelihood of the disc ever inverting (Heisinger *et al.* 2014). The development of such stabilization strategies could have significant implications on the design and control of unpowered flight in engineered robotic systems (Lentink & Biewener 2010; Paoletti & Mahadevan 2011), since it offers a way to alter the falling mode with little or no energy involved. One could envision, for example, a control mechanisms where the hole size is triggered by aerodynamical efforts on the body, prior to transitioning to a different mode. Our results may additionally shed light on the stability of gliding animals such as flying snakes that use body undulations, where they continuously vary the size of their S-shaped body, to actively stabilize their gliding motion (Jafari *et al.* 2014). Future research will focus on the falling behaviour of such S-shaped bodies and their passive stability.

Acknowledgement

This work is partially supported by the NSF grant CMMI 13-63404.

REFERENCES

ANDERSEN, A., PESAVENTO, U. & WANG, Z. J. 2005 Analysis of transitions between fluttering, tumbling and steady descent of falling cards. *J. Fluid. Mech.* **541**, 91–104.

AUGUSTE, F., MAGNAUDET, J. & FABRE, D. 2013 Falling styles of disks. *J. Fluid. Mech.* **719**, 388–405.

ERN, P., RISSO, F., FABRE, D. & MAGNAUDET, J. 2012 Wake-induced oscillatory paths of bodies freely rising or falling in fluids. *Annu. Rev. Fluid Mech.* **44**, 97–121.

FIELD, S. B., KLAUS, M., MOORE, M. G. & NORI, F. 1997 Chaotic dynamics of falling disks. *Nature* **388**, 252–254.

GAZZOLA, M., CHATELAIN, P., VAN REES, W. M. & KOUMOUTSAKOS, P. 2011 Simulations of single and multiple swimmers with non-divergence free deforming geometries. *J. Comput. Phys.* **230**, 7039–7114.

HEISINGER, L., NEWTON, P. K. & KANSO, E. 2014 Coins falling in water. *J. Fluid. Mech.* **742**, 245–253.

JAFARI, F., ROSS, S. D., VLACHOS, P. P. & SOCHA, J. J. 2014 A theoretical analysis of pitch stability during gliding in flying snakes. *Bioinspir. Biomim.* **9** (16), 025014.

JONES, M. A. & SHELLEY, M. J. 2005 Falling cards. *J. Fluid Mech.* **540**, 393–425.

LANDAU, L. D. & LIFSCHITZ, E. M. 1987 *Fluid Mechanics*. vol. 6. Pergamon Press.

LENTINK, D. & BIEWENER, A. A. 2010 Nature-inspired flight – beyond the leap. *Bioinsp. Biomim.* **5** (9), 040201.

LENTINK, D., DICKSON, W. B., VAN LEEUWEN, J. L. & DICKINSON, M. H. 2009 Leading-edge vortices elevate lift of autorotating plant seeds. *Science* **324**, 1438–1440.

MICHELIN, S. & LLEWELLYN-SMITH, S. G. 2009 An unsteady point vortex method for coupled fluid–solid problems. *Theor. Comput. Fluid Dyn.* **23**, 127–153.

MITTAL, R., SESHADRI, V. & UDAYKUMAR, H. S. 2004 Flutter, tumble and vortex induced autorotation. *Theor. Comput. Fluid Dyn.* **17**, 165–170.

MOFFATT, H. K. 2013 Three coins in a fountain. *J. Fluid. Mech.* **720**, 1–4.

PAOLETTI, P. & MAHADEVAN, L. 2011 Planar controlled gliding, tumbling and descent. *J. Fluid Mech.* **689**, 489–516.

ROGER, R. P. & HUSSEY, R. G. 1982 Stokes drag on a flat annular ring. *Phys. Fluids* **25** (6), 915–922.

THIELICKE, W. & STAMHUIS, E. J. 2014 Pivlab – towards user-friendly, affordable and accurate digital particle image velocimetry in matlab. *J. Open. Res. Softw.* **2** (1), e30.

WILLIAMSON, C. H. K. & GOVARDHAN, R. 2004 Vortex-induced vibrations. *Annu. Rev. Fluid Mech.* **36**, 413–455.

WILLMARTH, W., HAWK, N. E. & HARVEY, R. L. 1964 Steady and unsteady motions and wakes of freely falling disks. *Phys. Fluids* **7** (2), 197–208.

https://doi.org/10.1017/jfm.2016.432 Published online by Cambridge University Press